Available online at www.sciencedirect.com
SCIENCE DIRECT®
Advances in Space Research 34 (2004) 1281–1287
ADVANCES IN SPACE RESEARCH (a COSPAR publication)
www.elsevier.com/locate/asr

Deep space environments for human exploration

J.W. Wilson [a,*], M.S. Clowdsley [b], F.A. Cucinotta [c], R.K. Tripathi [a], J.E. Nealy [d], G. De Angelis [d]

[a] NASA Langley Research Center, 4 South Wright Street, MS 188B, Hampton, VA 23681-2199, USA
[b] NRC/NASA Langley Research Center, Hampton, VA 23681-2199, USA
[c] NASA Johnson Space Center, Houston, TX 77058, USA
[d] Old Dominion University, Norfolk, VA 23508, USA

Received 15 October 2002; received in revised form 9 October 2003; accepted 11 October 2003

Abstract

Mission scenarios outside the Earth's protective magnetic shield are being studied. Included are high usage assets in the near-Earth environment for casual trips, for research, and for commercial/operational platforms, in which career exposures will be multi-mission determined over the astronaut's lifetime. The operational platforms will serve as launching points for deep space exploration missions, characterized by a single long-duration mission during the astronaut's career. The exploration beyond these operational platforms will include missions to planets, asteroids, and planetary satellites. The interplanetary environment is evaluated using convective diffusion theory. Local environments for each celestial body are modeled by using results from the most recent targeted spacecraft, and integrated into the design environments. Design scenarios are then evaluated for these missions. The underlying assumptions in arriving at the model environments and their impact on mission exposures within various shield materials will be discussed.
Published by Elsevier Ltd on behalf of COSPAR.

Keywords: Galactic cosmic rays; Solar cosmic rays; Albedo particles; Trapped radiations

1. Introduction

Human missions beyond LEO will first be confined to the Earth's neighborhood and typically less than 100 days duration. With growing infrastructure and operations, astronauts will become career space workers with space career durations approaching from one to two thousand days over a 10-year career (Tripathi et al., 2002). This near earth development will provide infrastructure and experience for ventures beyond Earth's neighborhood first to Mars and beyond with missions of a 1000 days and more. The primary technology thrust to enable these developments are new propulsion systems and space radiation protection (O'Keefe, 2002). A triage of space-radiation health maintenance strategies includes crew selection, radiation shielding, choice of propulsion technology, operational planning, and biological countermeasures (Cucinotta et al., 2001). The control of the radiation insult to specific tissues is the first line of defense against adverse health effects. The physical insult can be controlled in a limited way through material arrangement and material choices in spacecraft design (Wilson, 2001).

Fundamental to radiation health risk assessment is the specification of the space environment and its transport through spacecraft materials to specific tissues. In the present paper, we discuss the development of software to evaluate the radiation environment anywhere in the solar system and at any projected time including evaluation of material shielding properties.

2. Deep space environments

There are two basic sources of space radiation in the solar system: galactic cosmic rays (GCR) leaking into

* Corresponding author. Tel.: +1-757-864-1414; fax: +1-757-864-8094.
E-mail address: john.w.wilson@nasa.gov (J.W. Wilson).

0273-1177/$30. Published by Elsevier Ltd on behalf of COSPAR.
doi:10.1016/j.asr.2003.10.052

the heliosphere from local interstellar space and solar particle events (SPE) associated with acceleration within the transition region (shock) between a coronal mass ejection (CME) and the local interplanetary medium (Reames, 1999). The inward diffusion of GCR into the solar system is countered by convective currents due to the outward expansion of the solar wind (Parker, 1965) resulting in an intensity reduction with decreasing helioradius. As to SPE, the CME volume expands with increasing helioradius reducing the shock intensity and resulting in less intense SPE. Very large SPE intensities result within the shock region. When a large body is encountered, the local GCR or SPE environment is effectively shielded in the direction of the body, new particles (especially neutrons) are produced in interactions with the body atmosphere and surface, and if there is an associated magnetic field with a large dipole component then the charged particles from neutron decay (proton and electron) may be trapped leading to intense radiation belts with maximum intensity near the magnetic equator (Divine and Garrett, 1983).

2.1. GCR environment

A solution of the appropriate Fokker–Planck equation was found by Parker (1965) in which the inward diffusion of galactic cosmic rays is balanced by the outward convection by the solar wind. The density of cosmic ions within the solar system, assuming spherical symmetry, is then related to the external density as

$$\mu(r,R) = \mu_0(R)\exp\left[-\int_r V(r')\,dr'/D(r',R)\right], \tag{1}$$

where $\mu(r,R)$ is the ion density at radial distance r and magnetic rigidity R (particle momentum per unit charge and determines the trajectory radius of curvature in a magnetic field), $\mu_0(R)$ is the density in interstellar space, $V(r)$ is the solar wind speed, and $D(r,R)$ is the diffusion coefficient (Balasubramanyan et al., 1967). The wind velocity and diffusion coefficient depend on the solar activity usually measured by a subjectively defined number of sunspots (Wolfe sunspot number) observed in the solar surface (see discussion in Wilson et al., 1999a) and there is a phase shift between sunspot number and modulation as the wind generated at the solar surface diffuses into the modulation cavity which extends far out into the solar system. The relation of sunspot number to the cosmic ray induced neutron monitor count rate in Deep River, Canada is shown in Fig. 1 during some of the more recent solar activity cycles with projections to 2022. The development of the statistical model of sunspot number and its application is discussed elsewhere (Wilson et al., 1999a, 2002a). We note that the cycle is reasonably well determined soon after solar minimum but chaos enters late in the cycle and great uncertainty enters in cycle projections across the solar minimum (Wilson et al., 1999a). The uncertainty from this chaos is not included in the current projections. The inverse relation of solar activity and cosmic ray intensity is clearly seen in the figure. A simplified version of the Parker diffusion model was implemented by Badhwar et al. (1994) in which the solar wind is held constant at 400 km/s and the diffusion coefficient is taken as a function of time and is correlated with the Mt. Washington neutron monitor count rate. The diffusion was found to be bimodal with unique dependence on the orientation of the solar magnetic dipole. Assuming an isotropic diffusion coefficient in which the diffusion coefficient generally increases with radial distance as $D(r,R) = D_0(R)r^s$, where s is on the order of 0–2, these assumptions lead to

$$\mu(r,R) = \mu_0(R)\exp\{-V_0(r_0^{1-s} - r^{1-s})/[(1-s)D_0(R)]\}, \tag{2}$$

where V_0, r_0, and $D_0(R)$ are the wind speed, size of the modulation cavity (50 to 100 AU), and diffusion coefficient at 1 AU, respectively. Eq. (2) is used to scale the modulated flux at 1 AU to arbitrary distance (Wilson

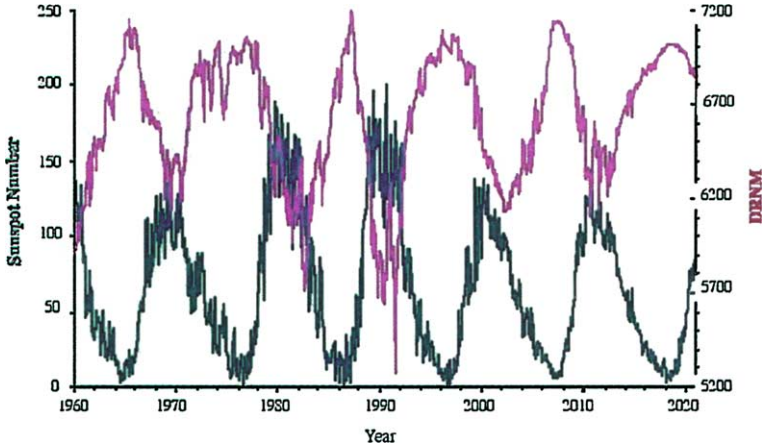

Fig. 1. Sunspot number and deep river neutron monitor countrate, actual and projected.

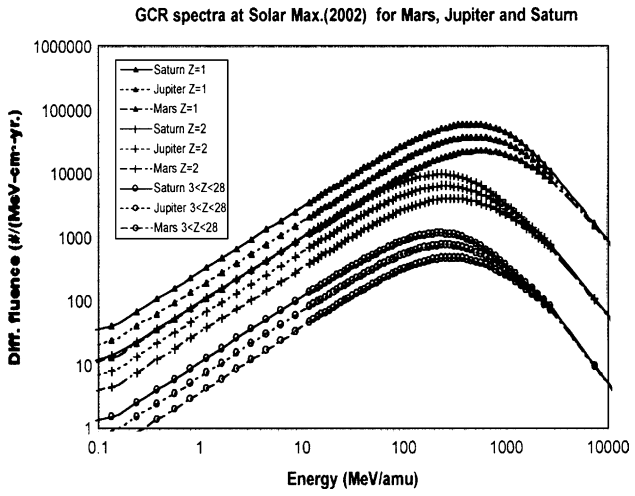

Fig. 2. GCR environment at solar maximum near Mars, Jupiter, and Saturn.

et al., 1999a). Modulation studies using various Pioneer, Voyager, and IMP spacecraft show variability of s with solar cycle for some restricted energy ranges but the gross behavior for all energies above 70 MeV per amu is well represented by $s = 0.5$ (Fuji and McDonald, 1997).

The solar modulation is less effective at solar minimum but the radial dependence during solar maximum is appreciable. The GCR environments near Mars, Jupiter, and Saturn are shown in Fig. 2 during the 2002 maximum in the solar cycle. It is clear that the lower energy GCR are less depleted at the larger heliocentric radii during solar maximum. This radial dependence will place additional demands on protection near solar maximum at large helioradii.

2.2. SPE environment

Solar cosmic rays or SPEs were first observed as sudden short-term increases in the ground level ionization rate. The close correlation with solar flare events first identified them as originating in the solar surface plasma with eventual release into the solar system (Meyer et al., 1956). Thus, it was assumed that the observation of solar surface phenomena would allow forecasting the possibility of such events (FAA, 1975). Modern opinion considers the particle acceleration region not to be on the sun at all (Reames, 1999). Rather large CMEs from active regions of the solar surface propagate into the interplanetary environment carrying along with them the local solar surface magnetic field frozen into the ejected mass (a good electrical conductor). There is a transition region (shock) between the normal sectored magnetic field structure of interplanetary space and the fields frozen into the ejected mass which forms a shock in which the interplanetary plasma is accelerated forming the solar particle event. The escape of the particles from the acceleration region is diffusion limited by particle–wave interaction with the interplanetary plasma so that a maximum intensity is implied. However, when the acceleration region passes the observation point the intensity is observed to increase by an order of magnitude to high levels in so-called shock events and no upper limit in intensity is known within the shock region (Reames, 1998). The SPE energies obtained in the acceleration process are related to the plasma density and velocity of propagation of the CME mass. To understand the SPE is then to understand the release of coronal mass and its propagation into interplanetary space relative to the observation point (Reames, 1999).

The SPE associated with Earth based ground level events (GLE) are intense at high energies and of greatest concern to human protection. The largest such event observed was the February 23, 1956 event with a GLE reaching 3600% over background. The third largest such event was the September 29, 1989 event reaching 370% over background as shown in Fig. 3. It has been demonstrated that a design environment taken as 4× September 29, 1989 assures that the even larger February 23, 1956 event would not have produced a significant biological consequence (Wilson et al., 1999b). We therefore use the 4× September 29, 1989 as a design environment. This is approximately the 99% environment of Xapsos et al. (1999). The radial dependence is problematic. Reames has suggested that very little SPE radial dependence may occur from Earth to Mars. Others have assumed Gauss law dependence. We have assumed an inverse dependence on helioradius to 2 AU and Gauss law beyond. Clearly the radial dependence of the SPE for missions near Earth Mars is of critical interest.

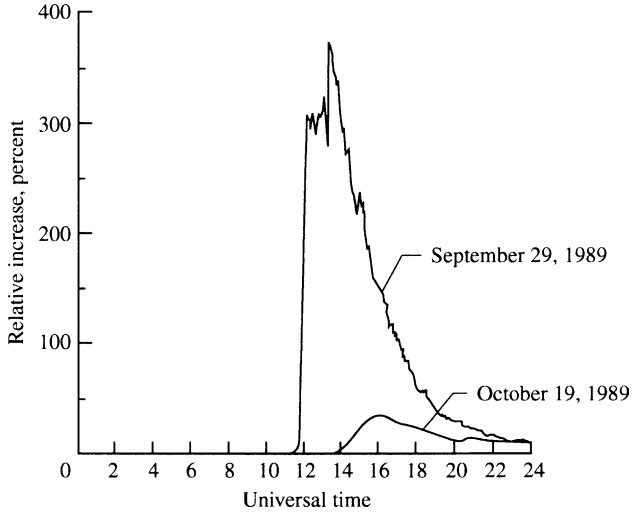

Fig. 3. Deep River neutron monitor count rates during the solar particle events of October 19 and September 29 of 1989.

3. Induced environments

The GCR and SPE are given by the above-discussed formalism in space that is free from any near bodies. As one approaches a large object such as a planet or a satellite, the ambient radiation field is disturbed by interaction with the near body. This interaction has several possible effects. In all cases, the produced neutrons diffuse into space providing a neutron albedo (to a lesser extent other particles as well). If there is an atmosphere then the neutrons on the surface of the body arise in part from interactions with that atmosphere and in part from those diffusing from below the local surface depending on the extent of the atmosphere. For example, it has been shown that neutrons on Mars surface with energies below 20 MeV are dominated by those produced in the bedrock or regolith (Wilson et al., 1999c). The water ice and CO_2 ice are less prolific in neutron production and becomes a feature of the neutron map as will be shown. If, in addition, the body has a dipole magnetic field then trapping regions can capture the neutron decay products allowing the buildup of intense electron and proton belts about the body as in the case of Earth and Jupiter. The Earth neighborhood has been discussed elsewhere and will not be further discussed herein (Wilson et al., 2002a).

3.1. Lunar surface environment

The GCR and SPE in the near Earth environment impact the lunar surface producing secondary particles, which diffuse from the surface into the local environment. In addition, the lunar mass shields the surface from directions intersecting the lunar terrain. On a smooth moon, the shielding effect is nearly a factor of two corresponding to all directions below the horizon. But, even local surface features can be used to protect human operations (Simonsen et al., 1990). In lunar orbit, the shadow cast by the lunar mass decreases and the neutron albedo decreases. The GCR environment on the lunar surface is shown in Fig. 4 at solar minimum and solar maximum. Similar results are shown in Fig. 5 for the solar particle event of September 29, 1989. Note, the particle intensity is completely dominated by the direct solar particles arriving from above the horizon. The difference between Figs. 4 and 5 is that the high-energy primary particles of the GCR are prolific in producing neutrons in comparison with the SPE event.

3.2. Mars surface environment

Galactic cosmic rays and solar energetic particles impact the martian atmosphere where interactions stop the low energy charged particles and modify the composition of the particle fields penetrating to the martian surface. The penetrating particle composition depends

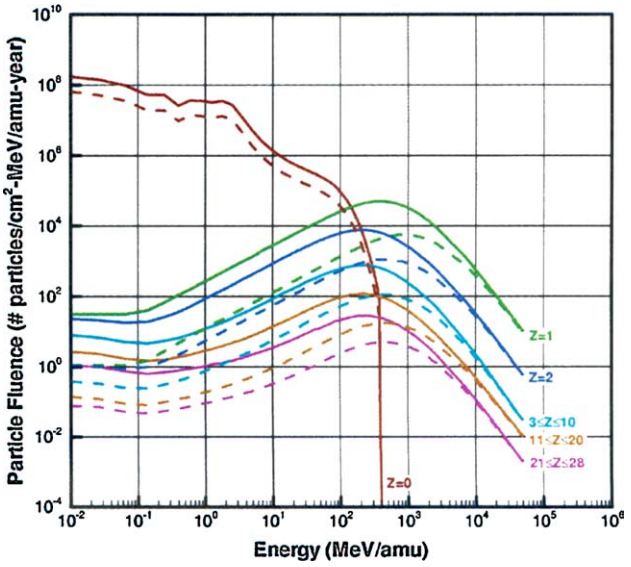

Fig. 4. Lunar surface induced GCR environment during the 1977 solar (full lines) and the 1990 solar maximum (dashed lines).

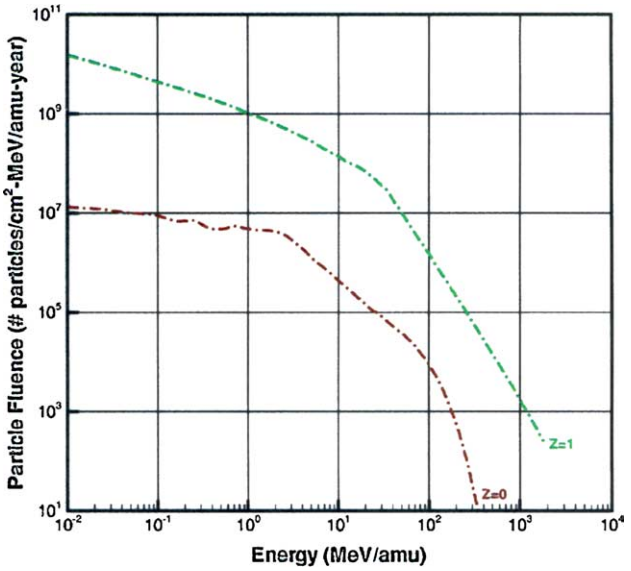

Fig. 5. The lunar surface environment during the September 1989 SPE.

on the amount of overhead atmosphere. On impact with martian surface materials provide additional modifications in the field including the production of neutrons which diffuse from the surface materials back into the atmosphere (Wilson et al., 1999c). The diffusive neutrons depend critically on the surface composition which in fact varies widely over the martian surface and is seasonally dependent. The computational geometry is shown in Fig. 6.

The martian atmosphere is modeled as CO_2 distributed according to the Marsgram model and the regolith composition is given by the Viking data with elevation from the Mars mapping missions. The seasonal depen-

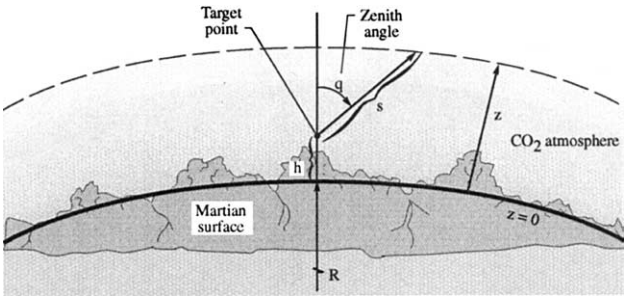

Fig. 6. Computational geometry for Mars surface environment (Simonsen et al., 1990).

dent water ice and CO_2 ice are also represented. The transport properties are represented by the HZETRN transport code and database with the low energy neutron transport handled by the computational procedures developed by Clowdsley et al. (2000).

Over regolith, the surface neutrons are dominated by those diffusing from the surface materials. This component is reduced over the CO_2 ice cap and becomes smaller still over water ice. This dependence is shown clearly in Fig. 7 where calculations of the total surface neutron flux spectra is shown along with the contribution from the overlying atmosphere (forward component in the figure). This will have some advantage in that the surface materials can be surveyed if the diffuse neutrons can be detected in low Mars orbit. Such an orbital model is under development and the ability to infer surface composition will be tested.

Galactic cosmic rays attenuation in the martian atmosphere with a buildup of secondary neutrons in reaching the surface is noted in features in Fig. 8. Clearly the high elevations are marked by intense surface neutrons where GCR impacts are high due to the reduced overhead atmosphere. The impact with the surface materials continues attenuation with greatly enhanced neutron production in regolith or bedrock (Wilson et al., 1999c), reduced in CO_2 ice, and especially in the water ice. Over regolith or bedrock, neutrons below 20 MeV diffusing from the surface materials into the atmosphere fully dominate the surface neutron environment giving enhanced and depleted neutron regions depending on composition. Hence, there are great differences in the surface neutron environment depending on the atmosphere overhead and the local surface materials. Polar surface materials change radically with season as seen in Fig. 8.

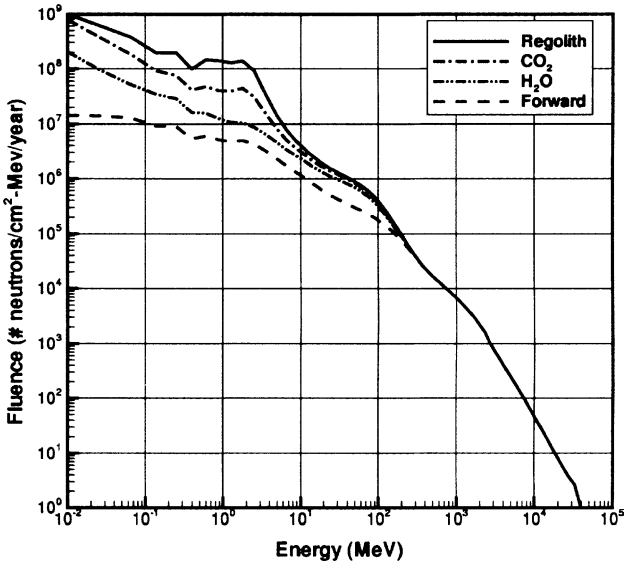

Fig. 7. Mars surface neutron environment with 16 g/cm^2 CO_2 overhead and various surface material compositions.

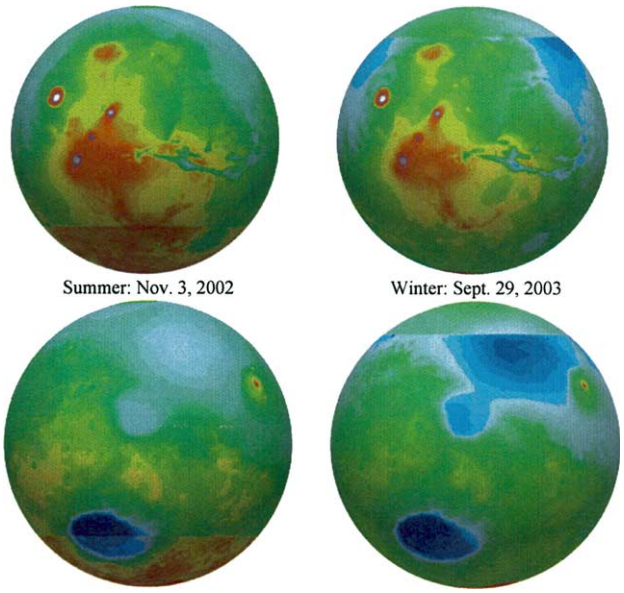

Fig. 8. Mars surface neutron environment above 10 MeV seasonal variation. Note that the color scale is not absolute and comparison of two hemispheres is only for qualitative features.

The degree of spatial resolution using neutron detectors in Mars orbit depends on the transmission characteristics of the Mars atmosphere. We anticipate that sufficient spatial resolution will allow detection of these features in Mars orbits of the Odyssey spacecraft and such a model is being developed. Note that these methods are distinct from the usual approach of detecting surface water where the neutron thermalization process is the marker. In this case, it is the Fermi motion and multiplicity of neutrons in nuclei of the surface materials that allow the >10 MeV neutrons to be a marker for surface properties. The atmospheric generated neutrons for the variable atmosphere is a confusing factor in interpretation of such measurements but the current computational models should allow such an analysis. An ideal instrument is available on the Odyssey spacecraft in its 400 km high inclination orbit for such studies (Prof. I. Mitrofanov, personal communication).

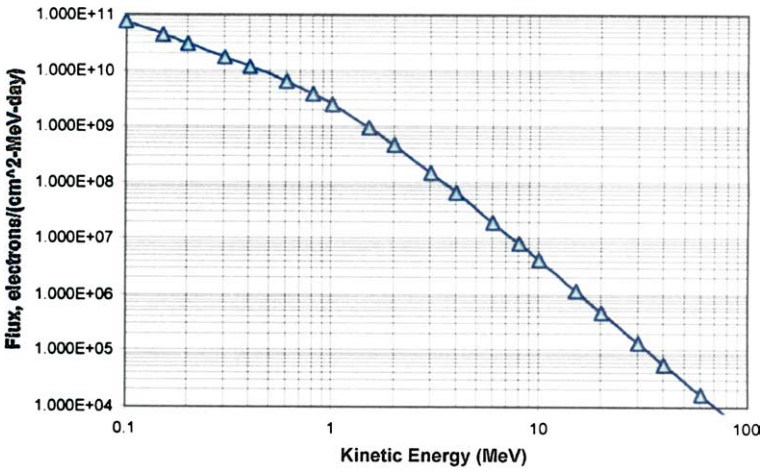

Fig. 9. Jovian electron environment near Callisto.

In addition to applications to Mars science, the models will allow the use of these models to assess the impact on human exposure and allow design considerations for all components in either surface operations, in lava tubes, or in Mars orbit.

3.3. Jupiter neighborhood

The solar wind generated convective currents produce less effects on the GCR near Jupiter relative to Earth. In addition, the jovian magnetic field traps particles with electron intensities to large distances from Jupiter (70 R_J). The electron flux spectrum near Callisto is shown in Fig. 9. Near a jovian moon, the intensities of all components are reduced except the induced neutron fields. We are developing an Anytime/Anywhere software package for use in mission analysis and an example of a mission from the Earth/Lunar L1 to Callisto and return is shown in Fig. 10 for a fixed mass of four shield materials. The mission starts near an assumed solar maximum (2045 AD) using the same projection model as in Fig. 1. The large exposure rates mid-mission are due to the jovian electron belts until arrival on the Callisto surface where there is shielding below the horizon. The continued increase of the environment on the return to L1 is due to decreasing solar activity. This software will soon include the Mars models presented in the previous section.

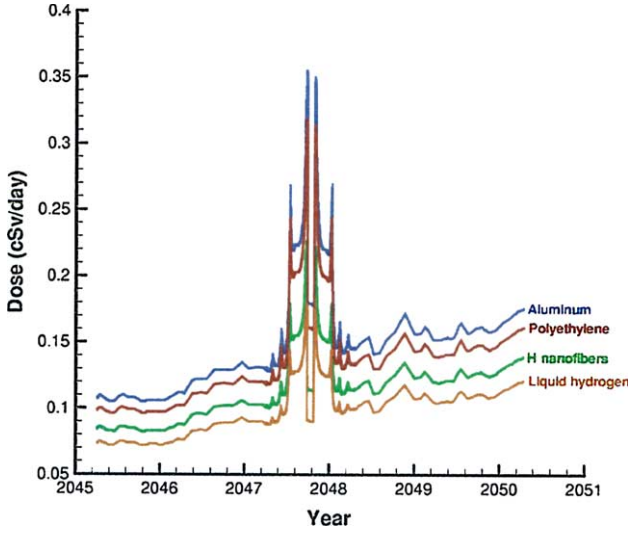

Fig. 10. Exposures within four materials of 4 g/cm^2 for mission to Callisto from L1.

4. Conclusions

The deep space environments developed for mission analysis use physical models to extrapolate the limited environmental data in both space and time. Induced fields are evaluated using high-speed transport models. Interesting dependence of local induced fields on atmosphere and ground composition are found which may be validated using Mars orbital data. The broader software being prepared will allow radiation exposure evaluation for arbitrary spectra in the future but limited to near Earth, near Jupiter, and interplanetary space for now. The near Mars environment will be added in the near future.

References

Badhwar, G.D., Cucinotta, F.A., O'Neill, P.M. An analysis of Interplanetary Space Radiation Exposure for various solar cycles. Radiat. Res. 138, 201–208, 1994.

Balasubramanyan, V.K., Bolt, E., Palmerira, R.A.R. Solar modulation of galactic cosmic rays. J. Geophys. Res. 72, 26–36, 1967.

Clowdsley, M.S., Heinbockel, J.H., Kaneko, H., Wilson, J.W., Singleterry, R.C., Shinn, J.L. A comparison of the multigroup and

collocation methods for solving the low-energy neutron Boltzmann equation. Can. J. Phys. 78, 45–56, 2000.

Cucinotta, F.A., Schimmerling, W., Wilson, J.W., Peterson, L.E., Badhwar, G.D., Saganti, P.B., Dicello, J.F. Space radiation cancer risks and uncertainties for Mars Missions. Radiat. Res. 156, 682–688, 2001.

Divine, N., Garrett, H.B. Charged particle distributions in Jupiter's magnetosphere. J. Geophys. Res. 88, 6889–6903, 1983.

FAA. Cosmic radiation exposure in supersonic and subsonic flights. Aviat., Space, & Environ. Med. 46, 1170–1185, 1975.

Fuji, Z., McDonald, F.B. Radial intensity gradients of galactic cosmic rays (1972-1995) in the heliosphere. J. Geophys. Res. 102 (A11), 24,201–24,208, 1997.

Meyer, P., Parker, E.N., Simpson, J.A. Solar cosmic rays of February, 1956, and their propagation through interplanetary space. Phys. Rev. 104, 768–783, 1956.

O'Keefe, S., Admistrator O'Keefe pitches his vision for NASA, 2002. Available from <http://www.spaceflightnow.com/news/n0203/27okeefe/>.

Parker, E.N. The passage of energetic charged particles through Interplanetary Space. Planetary Space Sci. 13, 9–49, 1965.

Reames, D.V., private communication, 1998.

Reames, D.V. Particle accereration at the sun and in the heliosphere. Space Sci. Rev. 90, 417–491, 1999.

Simonsen, L.C., Nealy, J.E., Townsend, L.W., Wilson, J.W., Space radiation for a martian habitat, SAE Tech Paper No. 891487, 1990.

Tripathi, R.K., Simonsen, L.C., Nealy, J.E., Troutman, P.A., Wilson, J.W., Shield optimization in simple geometry for the gateway concept, SAE 2002-01-2332, 2002.

Wilson, J.W., Kim, M.-H., Cucinotta, F.A., Badavi, F.F., Shinn, J.L., Tai, H., Badhwar, G.D., Atwell, W. Solar cycle variations and application to the space radiation environment. NASA TP-209369, 1999a.

Wilson, J.W., Cucinotta, F.A., Shinn, J.L., Simonsen, L.C., Dubey, R.R., Jordan, W.R., Jones, T.D., Chang, C.K., Kim, M.Y. Shielding from solar particle event exposures in deep space. Radiat. Meas. 30, 361–382, 1999b.

Wilson, J.W., Kim, M.Y., Clowdsley, M.S., Heinbockel, J.H., Tripathi, R.K., Singleterry, R.C., Shinn, J.L., Suggs, R., Mars surface ionizing radiation environment: need for validation, in: Workshop on Mars 2001: Integrated Science in Preparation for Sample Return and Human Exploration, Lunar and Planetary Institute, LPI Contribution No. 991, Houston, TX, October 2–4, 1999c.

Wilson, J.W. Overview of radiation environments and human exposures. Health Phys. 79, 470–494, 2001.

Wilson, J.W., Badavi, F.F., Kim, M.-H., Clowdsley, M.S., Heinbockel, J.H., Cucinotta, F.A., Badhwar, G.D., Atwell, W., Huston, S.L. Natural and induced environment in low Earth orbit. NASA/TM-2002-211668, 2002a.

Xapsos, M.A., Barth, J.L., Stassinopoulos, E.G., Burke, E.A., Gee, G.B., Space environment effects: Model for emission of solar protons (ESP) – cumulative and worst-case event fluences. NASA/TP-1999-209763, 1999.